ACS NANO

www.acsnano.org

ARTICLE

Clustered Regularly Interspaced Short Palindromic Repeats-Mediated Amplification-Free Detection of Viral DNAs Using Surface-Enhanced Raman Spectroscopy-Active Nanoarray

Jin-Ha Choi, Minkyu Shin, Letao Yang, Brian Conley, Jinho Yoon, Sang-Nam Lee, Ki-Bum Lee,* and Jeong-Woo Choi*

Cite This: *ACS Nano* 2021, 15, 13475−13485

Read Online

ACCESS | Metrics & More | Article Recommendations | Supporting Information

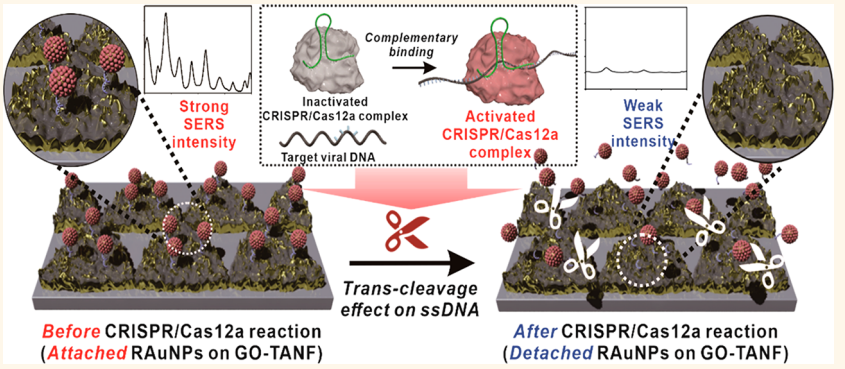

ABSTRACT: Nucleic acid biomarkers have been widely used to detect various viral-associated diseases, including the recent pandemic COVID-19. The CRISPR-Cas-based trans-activating phenomenon has shown excellent potential for developing sensitive and selective detection of nucleic acids. However, the nucleic acid amplification steps are typically required when sensitive and selective monitoring of the target nucleic acid is needed. To overcome the aforementioned challenges, we developed a CRISPR-Cas12a-based nucleic acid amplification-free biosensor by a surface-enhanced Raman spectroscopy (SERS)-assisted ultrasensitive detection system. We integrated the activated CRISPR-Cas12a by viral DNA with a Raman-sensitive system composed of ssDNA-immobilized Raman probe-functionalized Au nanoparticles (RAuNPs) on the graphene oxide (GO)/triangle Au nanoflower array. Using this CRISPR-based Raman-sensitive system improved the detection sensitivity of the multiviral DNAs such as hepatitis B virus (HBV), human papillomavirus 16 (HPV-16), and HPV-18 with an extremely low detection limit and vast detection range from 1 aM to 100 pM without the amplification steps. We suggest that this ultrasensitive amplification-free detection system for nucleic acids can be widely applied to the precise and early diagnosis of viral infections, cancers, and several genetic diseases.

KEYWORDS: *CRISPR-Cas12a, viral DNA, surface-enhanced Raman spectroscopy (SERS), triangle Au nanoflower, graphene oxide (GO), amplification-free detection*

Viral diseases have received immense attention in the medical and healthcare fields due to the high transmission rates and difficulty in curing. For example, severe acute respiratory syndrome coronavirus 2 (SARS-CoV-2) has rapidly and critically altered human life worldwide due to its highly contagious properties.[1−4]

Received: May 10, 2021
Accepted: August 2, 2021
Published: August 9, 2021

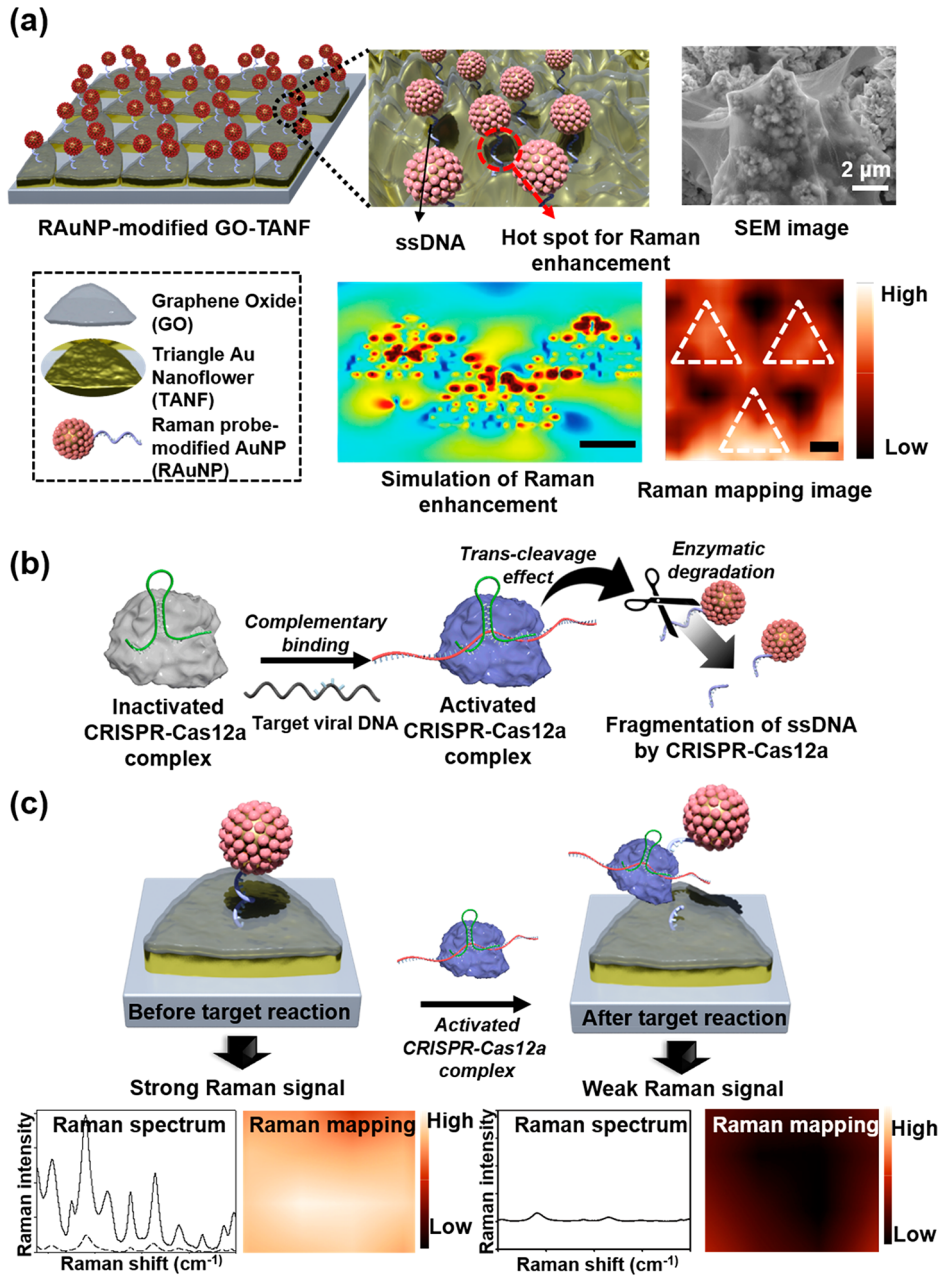

Figure 1. Schematic diagram illustrating the strategy to detect viral DNA using SERS-active graphene oxide (GO)/triangle Au nanoflower (GO-TANF). (a) GO-TANF with a Raman probe-modified Au nanoparticle (RAuNP) to enhance the SERS signal by generating a hot spot between RAuNP and GO-TANF. (b) Strategy of CRISPR-Cas12a-assisted viral DNA detection *via* the trans-cleavage effect of activated CRISPR-Cas12a by target viral DNA. (c) Pro-immobilized RAuNPs on the GO-TANF were separated from the surface owing to the degradation of ssDNA, and the maximized SERS intensity was reduced.

Especially, a prolonged incubation period without significant symptoms has permitted infected asymptomatic individuals to transmit the virus to noninfected individuals readily.[5−7] Over the past few decades, several diagnostic systems of viral diseases have been developed for early diagnosis. Traditionally, target nucleic acid amplification strategies such as polymerase chain reaction (PCR), recombinase polymerase amplification (RPA), and loop-mediated isothermal amplification (LAMP) have been widely used due to their high sensitivity and selectivity.[8−11] However, nucleic acid detection tools can become time-consuming and costly to employ, as they typically require multistep reactions, expensive reagents, well-trained personnel, and sophisticated instrumentation. Moreover, a quantitative analysis of these nucleic acid amplification techniques needs optimized methodologies to prevent diagnosis errors such as false-positive signals. Therefore, nucleic acid detection systems that overcome the limitations of conventional nucleic acid detection strategies are required by providing cost-effectiveness and high sensitivity for advancing their broad clinical applications.

In recent studies, clustered regularly interspaced short palindromic repeats (CRISPR)-associated nuclease-based analytical methods have been utilized to improve the sensitivity and simplicity of nucleic acid detection with fluorescent analytical methods.[12−16] CRISPR-associated nuclease 13a (Cas13a) and CRISPR-associated nuclease 12a (Cas12a) are

https://doi.org/10.1021/acsnano.1c03975
ACS Nano 2021, 15, 13475−13485

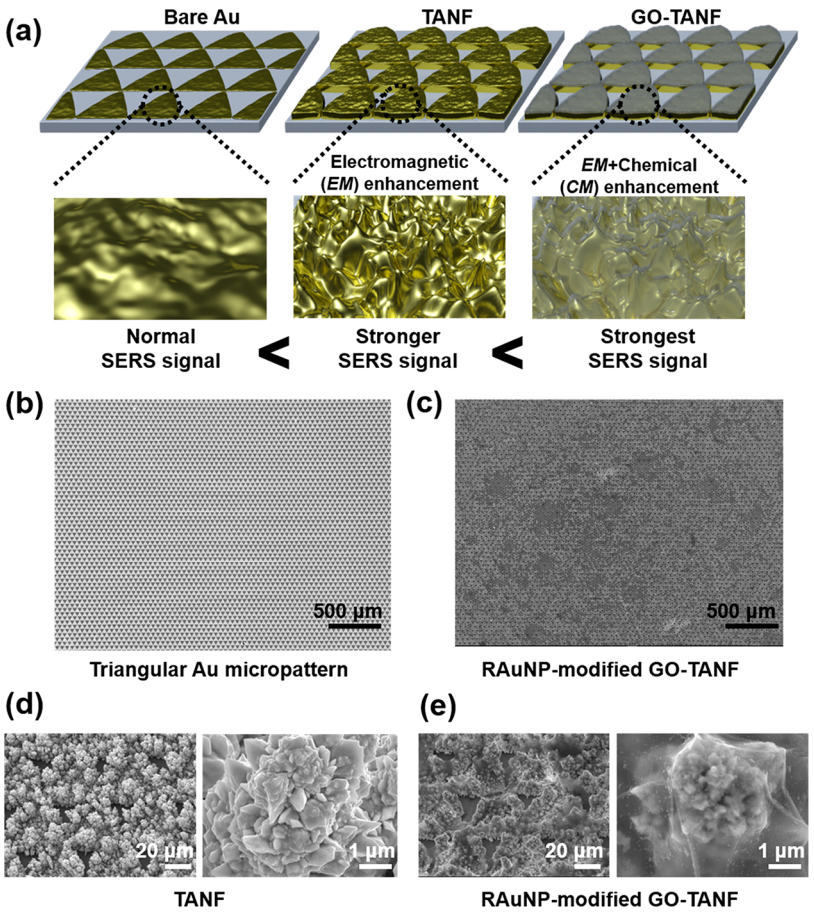

Figure 2. Morphology of the GO-TANF array. (a) Comparison of surface morphologies of bare Au, TANF, and GO-TANF for the electromagnetic (EM) and chemical (CM) enhancement of the SERS. (b, c) Scanning electron microscopy (SEM) images of (b) a triangular Au micropattern and (c) an RAuNP-modified GO-TANF with lower magnification. The scale bar is 500 μm. (d, e) SEM images of the surface of (d) a TANF and (e) an RAuNP-modified GO-TANF with higher magnification. Scale bars are 20 and 1 μm.

representative enzymes that have been applied to detect nucleic acids through their intrinsic enzymatic cleavage properties (trans-cleavage or collateral effect) of single-strand RNA or DNA during activation *via* recognition of target nucleic acids.[17,18] These methods demonstrated sequence-specific and sensitive RNA and DNA detection *via* trans-cleavage of an ambient single-stranded nucleic acid probe with target amplification. Due to the programmability of CRISPR-Cas RNA guides, these methodologies are easily tailored to detect specific target sequences. However, most CRISPR-Cas-based detection methods still rely upon initial amplification steps, which may suffer from complicated steps and false-positive signals, resulting in additional time and reagents.

Raman spectroscopy is a powerful analytical method to identify biomarkers' specific chemical structures through scattering phenomena with incident light. However, Raman signal intensity is typically too weak to detect an infinitesimal level of viral DNA/RNA in the real sample, which is typically required for an early diagnosis. On the other hand, surface-enhanced Raman scattering (SERS) is a signal-enhancing technique that manipulates surface plasmon effects on metal surfaces and further improves the detection capabilities of Raman spectroscopy to measure low concentrations of biomolecules.[19] Several nanomaterials with diverse shapes (*i.e.*, circle, triangle, *etc.*) could be utilized for sensitive detection to maximize the SERS effect. In particular, strong electromagnetic (EM) fields related to the plasmon resonance properties of noble nanomaterials are used to increase the Raman vibrational signals from target analytes.[20−23] With possible enhancement factors up to 10^{14}, SERS analytical methods represent an exceptionally sensitive detection method with optimized nanomaterials.[24−27] Having their advantages, SERS-integrated amplification-free CRISPR-Cas9 biosensors have been shown to detect multidrug-resistant bacteria with femtomolar sensitivity.[28] However, rapid, sensitive, and selective detection of viral biomarkers is still urgent in preparing for future pandemics.

In this study, we report the development of an amplification-free viral DNA biosensor with a CRISPR-Cas12a-assisted SERS analytical system (Figure 1). Our system was developed by synthesizing a SERS-active graphene oxide (GO)/periodic triangle Au nanoflower (TANF) array with Raman probe-functionalized Au nanoparticles (RAuNPs) (Figure 1a). Our advanced viral DNA sensor design provides an ultrasensitive system by maximizing SERS signal intensity to omit the nucleic acid amplification used in other detection systems. Here, the TANF array, which is composed of Au microstructures (periodic triangle Au micropattern) and nanostructures (Au nanoflower structures), was synthesized to enhance the SERS signal. Both microsized triangles and nanoflower structures were anticipated to enhance the Raman signal due to highly concentrated surface electrons on their surface. Besides, GO on the TANF surface promoted chemical (CM) enhancement through charge-transfer mechanisms.[29−32] Using this phenom-

https://doi.org/10.1021/acsnano.1c03975
ACS Nano 2021, 15, 13475−13485

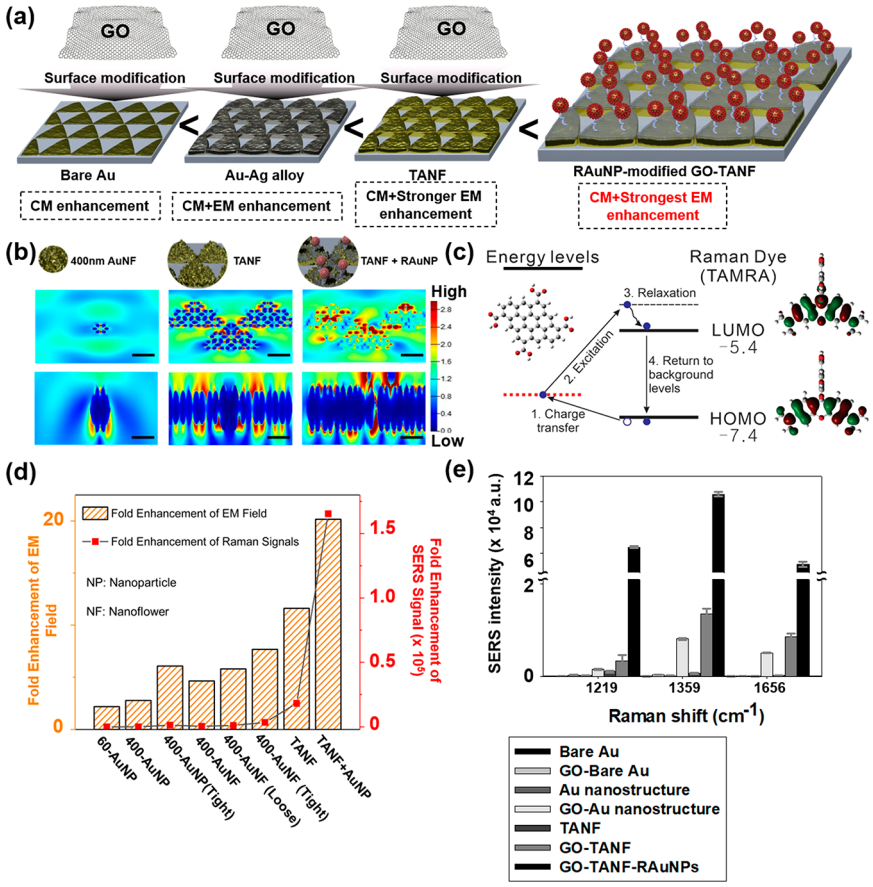

Figure 3. Enhancement of SERS intensity of RAuNPs on the GO-TANF array. (a) Schematic diagram of the most-enhanced substrate by the CM and EM enhancement of the bare Au, Au−Ag alloy, TANF, and RAuNP-modified GO-TANF. (b) Finite-difference time-domain (FDTD) simulation for EM enhancement of a 400 nm-sized AuNPs assembly, TANF, and RAuNP-modified TANF. (c) Simulation of the CM enhancement effect of the Raman probe (TAMRA) on the GO. (d) Bar chart of each substrate's EM enhancement effect (60 nm-sized AuNP, 400 nm-sized AuNP, 400 nm-sized AuNPs with denseness, 400 nm-sized AuNF, 400 nm-sized AuNFs with looseness, 400 nm-sized AuNFs with denseness, TANF, and RAuNP-modified TANF, respectively) from the FDTD simulation. (e) SERS intensity of each substrate (bare Au, GO-modified Au, Au nanostructure, GO-modified Au nanostructure, TANF, GO-TANF, and RAuNP-modified GO-TANF, respectively) from the experimental results of the Raman spectrum.

enon, RAuNPs, which showed enhanced Raman signal, were connected to the GO-TANF by the ssDNA for the maximized SERS effect, and the SERS signal intensity resulted in a significant difference between the presence and absence of viral DNA through the trans-cleavage reaction of activated CRISPR-Cas12a (Figure 1b and c). The activation of CRISPR-Cas12a complexes by target viral DNA could cleave ambient single-stranded DNA (ssDNA), which is connected between GO-TANF and RAuNPs. Therefore, this system could demonstrate rapid, multiplex, and quantitative detection of attomolar concentrations of viral DNA within 20 min.

RESULTS/DISCUSSION

Characterization of the SERS-Sensitive GO-TANF Array. The optimal design for the induction of strong EM enhancement is crucial for the improvement of detection sensitivity. To this end, regions with high SERS enhancement (known as hot spots) were designed by tuning both micro- and nanosized Au structures to provide areas where Raman enhancement increased dramatically (Figure 2a). First, triangle-shaped microstructures can generate hot spots at their structural boundaries, such as edges and vertices. Also, contact points between adjacent triangle microstructures can also provide hot spots.[33] For this purpose, a triangle-shaped Au micropattern array was fabricated by photolithography, forming overlaid small vertices, with a length of 1 μm, encompassing three adjacent Au triangles (Figure S1). Second, it has been reported that rough-faced metal nanostructures can also provide hot spots to increase SERS signal intensity.[34] Thus, Au/Ag co-electrodeposition was employed to fabricate Au "nanoflower" structures, which provided a rough physical surface to enhance EM phenomena. The Ag was subsequently removed during etching at the Au/Ag substrate, and Au formed a rough-shaped nanostructured surface, named a Au nanoflower (Figure S2). Third, GOs have been shown to serve as additional CM enhancement of Raman signals. As a result, both EM and CM were employed by immobilizing GO on the TANF surface. Lastly, a Raman probe was functionalized on the surface of Au nanoparticles (AuNPs), further bound to the GO-TANF array by heterobifunctional ssDNA, which modified thiol and amine groups. Therefore, the Raman probe was placed at the particular area between the AuNP and GO-TANF, where the EM and CM effects were the strongest on the GO-TANF array. Through these strategies, the SERS signal intensity of the Raman probe was drastically enhanced. On this substrate, the target sequence of viral DNA acted as an activator for the CRISPR-Cas12a complex's trans-cleavage reaction, which can cleave ssDNA randomly upon binding to

https://doi.org/10.1021/acsnano.1c03975
ACS Nano 2021, 15, 13475−13485

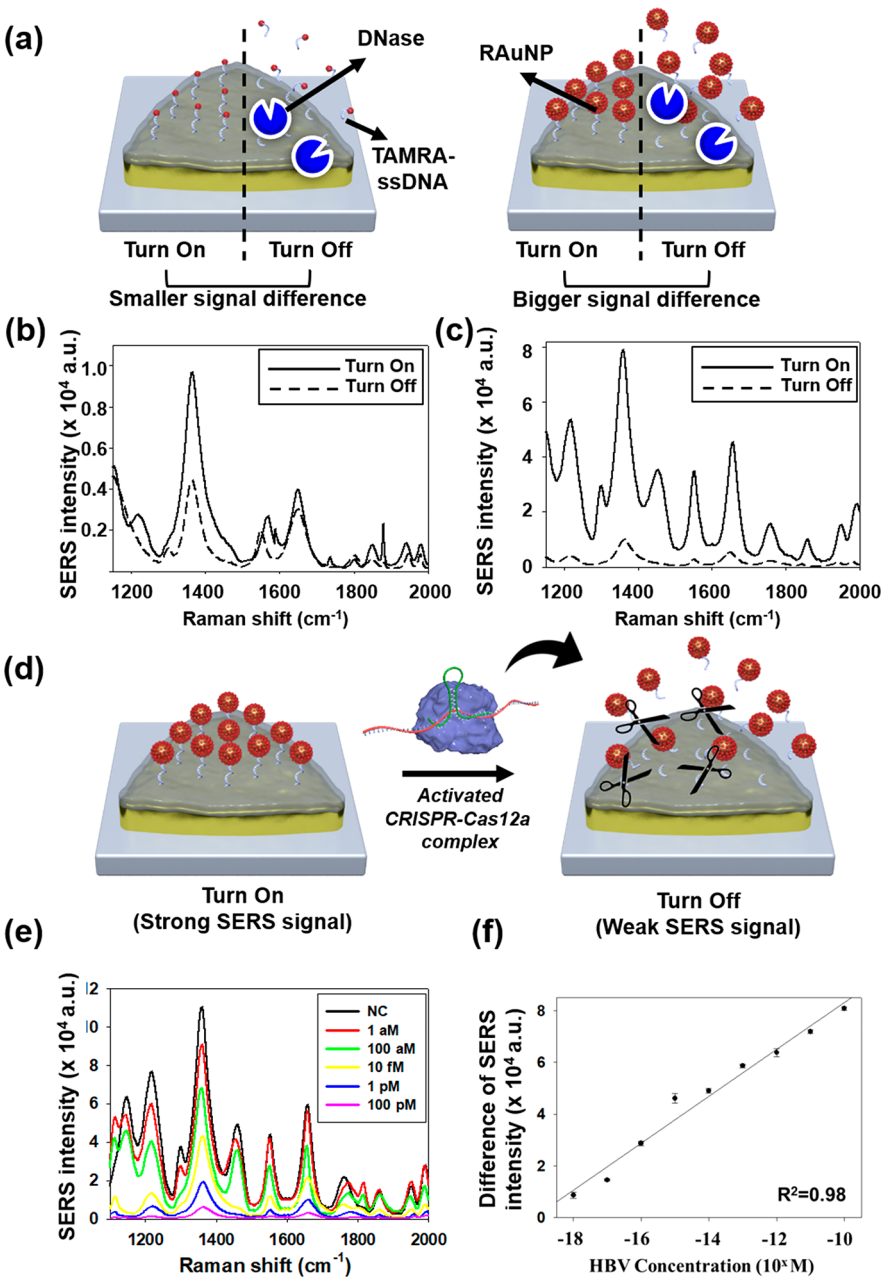

Figure 4. Highly sensitive measurement of hepatitis B virus (HBV) DNA on the RAuNP-modified GO-TANF array by CRISPR-Cas12a-based ssDNA degradation. (a) Schematic diagrams of ssDNA degradation and SERS signal difference between TAMRA-ssDNA-modified GO-TANF and RAuNP-modified GO-TANF by DNase. (b) Raman spectrum of the TAMRA-ssDNA-modified GO-TANF and (c) RAuNP-modified GO-TANF before and after DNase treatment (d) Schematic diagram of turn-on and turn-off states by the trans-cleavage effect of the CRISPR-Cas12a complex on the RAuNP-modified GO-TANF array. (e) Raman spectrum of the RAuNP-modified GO-TANF array with varying concentrations of HBV DNA, ranging from 1 aM to 100 pM, respectively. (f) Linear relationship of the decrease of SERS intensities and the concentrations of HBV DNA, corresponding to (e).

target DNA (Figure 1c). The ssDNA bridge between RAuNPs and GO-TANF was cleaved, and the SERS signal intensity from the RAuNPs drastically decreased. Target viral DNA was quantified rapidly and sensitively without a nucleic acid amplification step *via* this CRISPR-Cas12a-based enzymatic reaction.

To this end, we fabricated large-scale homogeneous Au microsized triangle patterns by photolithography, having precisely tuned periodic structures (Figure 2b). Afterward, an Au/Ag plating solution (atomic ratio of 1:1) was electrodeposited on the Au pattern and underwent chemical etching to remove Ag for the development of a rough-faced Au nanostructure (Figure 2c). We then characterized the surface morphology of the TANF structure by scanning electron microscopy (SEM), confirming a rough, flower-like structure, likely induced through etching of Ag during postprocessing (Figures 2d, S3, S4, and S5). The EM enhancement of Au nanoflowers provided a large Raman-sensitive area to improve sensitivity. In contrast, nondeposited, Au deposited, and Au/Ag co-deposited triangle Au microstructures exhibited smoother surfaces than the TANF array (Figure S3). Subsequently, GO was coated on the TANF array to promote

https://doi.org/10.1021/acsnano.1c03975
ACS Nano 2021, 15, 13475−13485

the CM enhancement of the Raman signal (Figure 2e and Figure S4b). The shape of GO-coated Au nanoflowers became indistinct as characteristic sheet-like structures from GO appeared on the surface of the GO-TANF array. To analyze the atomic composition of the GO-TANF array more clearly, energy-dispersive X-ray spectroscopy (EDS) mapping was conducted (Figure S6). The quantity of Ag was drastically decreased after the treatment of the Ag etching solution.

Enhancement of the SERS Signal Intensity by the GO-TANF Array and RAuNPs. As depicted in Figure 1c, even a low level of viral DNA could be measured due to the SERS signal enhancement using the GO-TANF array and RAuNPs. For the SERS signal enhancement, four different designs were integrated into one substrate. First, EM enhancement was induced by the rough-faced Au nanoflower structure. To verify the SERS signal enhancement effect on the rough-faced Au nanoflower substrate, the D and G bands of the immobilized GO were measured on three different Au structures: bare Au-coated glass, Au electrodeposited Au-coated glass, and Au nanoflower-modified Au-coated glass (Figure 3a). By comparing the SERS signal intensities of D (1350 cm^{-1}) and G (1600 cm^{-1}) bands (Figure S7), the GO-modified Au nanoflower exhibited high signal intensities for both D and G bands compared to GO-modified bare Au-coated glass. On the other hand, Au electrodeposited Au-coated glass showed SERS signals approximately half of the value of GO-modified Au nanoflowers. The rough surface of the Au nanoflower was caused by the vacancy of Ag that was eliminated by the oxidative etching (*e.g.*, $Ag + 2HNO_3 = Ag^+ + NO_2 + NO^{3-} + H_2O$). Moreover, as the ratio of deposited Au:Ag could confer differences in EM signal enhancement (Figures S8 and S9), various conditions of the Au−Ag concentration ratio were tested, and it was found that 1:1 (atomic ratio) was the most efficient mixed solution for the SERS signal enhancement. In comparison, a greater concentration of Ag resulted in insufficient enhancement from the small amount of remaining Au on the substrate. On the other hand, Au nanostructures alone do not have a rough surface, resulting in a smaller enhancement effect than the Au nanoflower structure. In addition, Au nanoflowers could increase the active surface of SERS signal enhancement within the limited laser spot size (about 1 μm) of the Raman instrument. Thus, both rough surface and increased surface area of Au nanoflowers provided an excellent SERS signal enhancement substrate.

Second, a triangle Au microstructure could be another critical factor for signal enhancement by providing strong signal generation at the vertices and edges of Au microstructures. Moreover, overlaid small points between individual Au microstructures could also be a source of signal enhancement. As predicted, the SERS signal showed the highest intensity at the vertex on the TANF array (Figure S10). This was also confirmed by performing three-dimensional finite-difference time-domain (FDTD) simulations on the TANF array and monitoring the EM field at different planes (Figure 3b and d). The FDTD simulation highlights the importance of our hierarchical nano/microstructures in improving SERS signals, validates our hypothesis, and further determines our TANF-based biosensors' sensitivity. Third, CM enhancement through charge-transfer mechanisms could also be confirmed by the simulation of the Raman probe (TAMRA) on the surface of GO (Figure 3c).

Lastly, we further incorporated Raman probes to provide sensitive and selective signals for specific biomolecular detection with strong SERS signals. More specifically, we utilized 5-TAMRA-functionalized AuNP as a Raman probe, which showed greater SERS signal intensity owing to the EM effect on the AuNP (Figure 3a). This Raman probe was attached to the GO-TANF array *via* ssDNA, whose length was small enough to generate a hot spot effect between AuNPs and GO-TANF (below 4 nm). The functionalization of both 5-TAMRA and ssDNA was confirmed by measuring the fluorescence intensities (Figure S11). Through the EM and CM enhancement from the GO-TANF and AuNP, SERS signals of the 5-TAMRA showed the strongest spectral intensity compared to other cases (Figure 3e). All three specific Raman peaks of TAMRA (1219, 1359, and 1656 cm^{-1}) exhibited the greatest enhancement effects. Notably, AuNP played a significant role in amplifying the SERS signals, over 10 times higher than the TAMRA-modified ssDNA alone. Taking advantage of this improved Raman-sensitive system, the decrease of the Raman intensities was further confirmed by using DNase, which induced DNA degradation between the Raman probe and the GO-TANF array (Figure 4a). In applying RAuNPs as a Raman probe, the SERS signal intensity was drastically reduced due to the degradation of ssDNA (Figure 4b and c). On the contrary, TAMRA-modified ssDNA was dismantled with a smaller decrease of the SERS signals, around half the intensity compared to SERS signals after ssDNA degradation in both cases. The absolute values of both Raman intensities showed similar levels. In other words, maximizing the SERS signal intensity could provide a more sensitive system for detecting the enzymatic cleavage reaction.

Ultrasensitive Detection of Viral DNA by the Activated CRISPR-Cas12a on RAuNP-Modified GO-TANF. Our GO-TANF array was developed to enhance the SERS signal intensity using optimized EM and CM enhancement effects. In addition, our advanced Raman probe, which is TAMRA-functionalized AuNPs (RAuNPs), could induce a synergistic increase in SERS signal intensity with the GO-TANF array. To verify the SERS enhancement effect, a 10-nucleotide-length ssDNA, which is short enough to produce SERS of the Raman probe by GO-TANF and AuNPs, was provided as a degradable target by the activated CRISPR-Cas12a complex by target viral DNA (Figure 4d). On the other hand, the absence of target viral DNA did not show a trans-cleavage effect of the CRISPR-Cas12a complex. As such, the corresponding Raman peaks remained primarily unchanged at a high signal intensity. To verify the correlation of decrease of SERS signal intensity with dissociation of RAuNPs, we then measured the Raman intensities after applying DNase to the RAuNPs attached to GO-TANF and confirmed the radical decrease of the signal. The activated CRISPR-Cas12a complex showed similar degradation with DNase against all the ambient ssDNA (Figure S12).

As a proof-of-concept, the hepatitis B virus (HBV), a DNA virus that causes severe liver infection, was selected as a model viral DNA target. As shown in Figures 4e,f and S13, HBV DNA was successfully measured with high selectivity and ultrahigh sensitivity, ranging from 1 aM to 100 pM. Most of the fluorescence-based nucleic acid-sensing system by the CRISPR enzyme has been utilized in the target amplification process through the LAMP and RPA due to the target's sensitive detection. On the other hand, we achieved a similar detection level of target DNA (1 aM) to the presented CRISPR-based viral detection methods with high linear regression (R^2 = 0.98 at 1656 cm^{-1}) without an amplification process. Additionally,

https://doi.org/10.1021/acsnano.1c03975
ACS Nano 2021, 15, 13475−13485

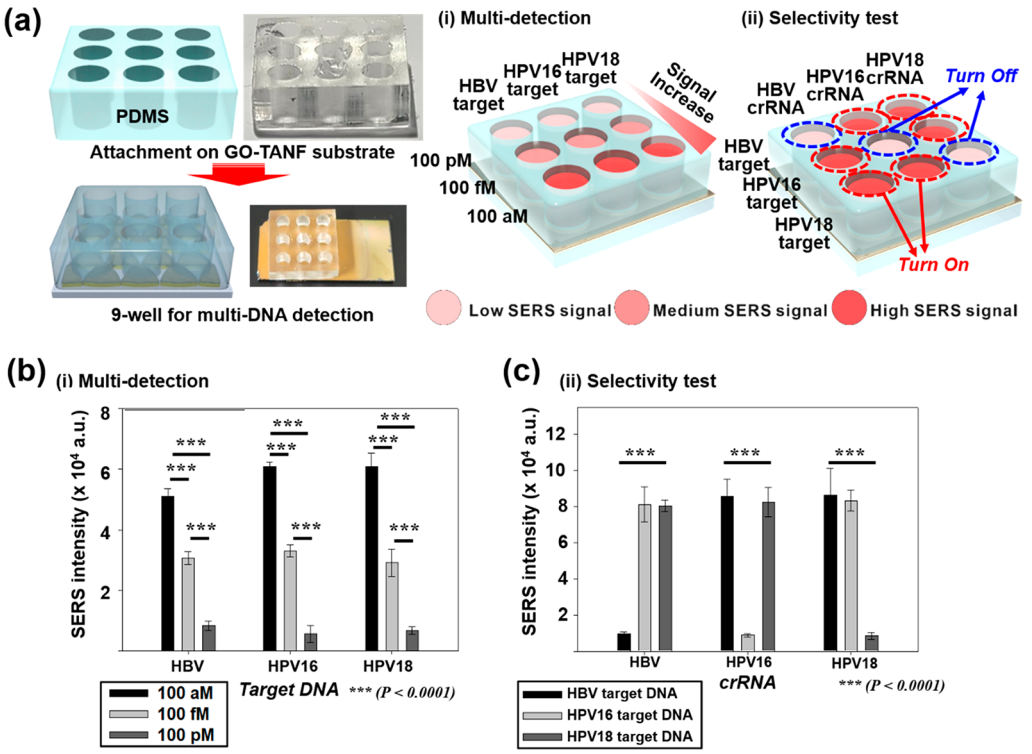

Figure 5. Multiplexed detection of viral DNA on a GO-TANF array by the activated CRISPR-Cas12a complex. (a) Schematic diagram of the multiwell system for (I) multiplex viral DNA detection and (II) specificity test of each target DNA, including HBV, human papillomavirus 16 (HPV16), and human papillomavirus 18 (HPV18), respectively. (b) Raman intensities at 1359 cm^{-1} for multiplex viral DNA detection at three different target DNA concentrations (100 aM, 100 fM, and 100 pM). (c) Raman intensities at 1359 cm^{-1} for the target specificity of a nine-well GO-TANF chip. The target concentrations were 100 pM.

the required time for the detection is reduced to only 20 min from more than 1 h of the existing Cas-based detection for attomolar detection of target oligonucleotides. Dissociation of RAuNPs on the GO-TANF array was also verified in Figure S14, after 20 min of applying target DNA (1 nM) as an electron microscope image. Our approach may address critical issues such as high cost, tedious procedures, and false-positive events in conventional viral detection techniques with the development of miniaturized and low-cost Raman instruments.

Multiplexed Viral DNA Detection on a Multiwell GO-TANF Platform. Developed CRISPR-Cas12a-based biosensors have several clear advantages, including sensitive (aM level), selective (negative signals from other nonspecific targets), and rapid detection (20 min) compared to conventional biosensing systems. Moreover, this system could facilitate the detection of multiviral DNA by applying different CRISPR RNA (crRNA) sequences, which is crucial for the scalability of high-throughput testing. As a proof-of-concept study, multiwell polydimethylsiloxane (PDMS) structures were rendered by a three-dimensional (3D) printing technique and attached to the GO-TANF array (Figure 5a) by plasma treatment. Specifically, the multiwell system consisted of nine independent wells (3 by 3) to detect three different viral DNAs, including HBV, human papillomavirus 16 (HPV16), and human papillomavirus 18 (HPV18), respectively. In the case of HBV, early-stage detection is one of the critical issues for health surveillance, as a delayed diagnosis can lead to chronic hepatitis, cirrhosis, and primary liver cancer. In addition, early detection of HPV can identify precancerous lesions in the cervix, preventing cervical cancer in adult women. To verify three different target detections at an early stage, we applied CRISPR-Cas12a with different crRNAs before the injection of target DNA on the preimmobilized RAuNPs on GO-TANF. As each detection in the multiplexing system was based on individual crRNA−target DNA complementary reactions, all the concentrations of RAuNPs immobilized on GO-TANF were kept identical in each well. After applying the crRNA-Cas12a complex to the well containing GO-TANF, three different concentrations of each target (HBV, HPV16, and HPV18) were used, including high (100 pM), medium (100 fM), and low (100 aM) concentrations, for 20 min, respectively. In Figure 5b, multiplexed detection succeeded with three different concentrations (100 aM, 100 fM, and 100 pM). Interestingly, despite differences in DNA sequences between different viral strands, the Raman intensities of all equal concentrations were similar. Moreover, each target DNA could be detected with a specifically designed crRNA-Cas12a complex at high precision based on the decreased SERS signal intensity (Figure 5c). Different viral DNA targets could be measured in this sensing system by designing specific complementary crRNA in a highly selective and sensitive manner, desired for probing the heterogeneous viral sequences (*e.g.*, mutants) in clinical applications.

CONCLUSIONS

In this study, the CRISPR-Cas12a-based viral DNA biosensing system was developed by integrating microfabrication into nanomaterials-enabled SERS applications for maximized SERS signal intensity without integrating a target amplification step. Using this system, low concentrations of viral DNA, as low as 1 aM, were successfully measured within 20 min by reducing the

https://doi.org/10.1021/acsnano.1c03975
ACS Nano 2021, 15, 13475−13485

Table 1. Current CRISPR-Based Amplification-Free Biosensors

detection technique	CRISPR enzyme	target	limit of detection	linear dynamic range	required time	multiplex (Y/N)	ref
electrochemical detection	Cas13a	miR-19b	10 pM	10 pM−1 nM	70 min	N	35
electrochemical detection	Cas12a	HPV-16	50 pM	100 pM−100 μM	30 min	N	36
field-effect transistor	Cas9	genomic DNA	1.7 fM		30 min	N	37
fluorescent detection	Cas13a	miR-17	1 pM	1 pM−10 nM	30 min	N	38
electrochemical detection	Cas12a	parvovirus B19	100 fM	100 fM−10 nM	30 min	N	39
electrochemiluminescence detection	Cas13a	miR-17	1 fM	1 fM−100 pM	90 min	N	40
electrochemical detection	Cas13a	miR-19b, 20a	2−18 pM		210 min	Y	41
fluorescent detection	Cas12a	BRCA-1	0.34 fM	1 fM−100 pM	30 min	N	42
electrochemical detection	Cas12a	DENV DNA	100 fM	100 fM−10 nM	30 min	N	43
electrochemiluminescence detection	Cas12a	HPV-16	0.48 pM	1 pM−10 nM	70 min	N	44
microdroplet fluorescent detection	Cas13a	miR-17, 16S rRNAs, SARS-CoV-2 RNA	10 aM	10 aM−100 fM	70 min	N	45
surface-enhanced Raman scattering	Cas12a	HBV, HPV-16, HPV-18	1 aM	1 aM−100 pM	20 min	Y	this work

SERS signal intensity. The advantages of the suggested system for viral DNA detection can be summarized in two ways. First, regarding the sensing substrate, it allowed ultrasensitive detection of viral DNA without nucleic acid amplification, which could induce time-consuming, cost-ineffective, and false-positive detection. The amplification process is necessary for polymerase-based methods when nucleic acid quantity is minimal. To overcome these limitations, we improved the sensitivity of the sensing substrate by applying a sensitive detection strategy. In detail, we designed triangle Au microstructures to provide the specific area of high electron density at the vertex where three independent Au triangles were overlaid and formed 1 μm-sized small regular triangles periodically. Moreover, rough-faced Au nanoflower structures were positioned on the triangle using the electrodeposition of Au and Ag and partially etching Ag. These rough-faced Au nanoflowers facilitated EM enhancement by forming a hot spot region. Second, regarding the sensing strategy, we expected that CRISPR-Cas12a-based enzymatic cleavage could improve the sensitivity from other DNA detection strategies owing to its trans-cleavage reaction properties. To maximize the signal change of the SERS signal intensity by activated CRISPR-Cas12-based ssDNA degradation, enhanced Raman probes (RAuNPs) were attached to GO-TANF by ssDNA. When the activated CRISPR-Cas12 complex degraded the ssDNA as a bridge, Raman intensities were drastically reduced in proportion to detached RAuNPs from the GO-TANF. This strategy provided a simple and ready-to-use detection approach because it does not require any poststeps such as labeling and washing after the target reaction.

Taken together, our developed CRISPR-Cas12-based biosensing system could provide a very promising and high-potential system for rapid, simple, precise, and ultrasensitive detection of viral DNA. This CRISPR-based amplification-free DNA detection system showed the best performances, such as a low limit of detection (LOD), wide linear dynamic range (LDR), short reaction time, and multidetection (Table 1). On top of these advantages, other DNA targets could also be measured by simply changing the crRNA sequence. It will enable us to get more specific information regarding diseases, such as predicting the latency and progression of diseases by measuring the level of genomic DNA or cell-free DNA (cfDNA). In addition to DNA targets, other representative biomarkers, including RNA or protein, might be detected by applying Cas13a protein for RNA targets and aptamers for proteins. In this respect, the developed system has excellent versatility and could be used for point-of-care testing to detect various biomarkers. Nonetheless, there are some challenges, such as minimizing the Raman instrument and its relatively high price for a portable and highly accessible system. In addition, there should be optimization steps for the enhancement of SERS signal intensity and sensitivity of the targets. For example, the optimal size of the AuNP and triangle Au microstructure could improve the sensitivity of the sensor. Furthermore, including shortening the assay time and reduction of the detection limit may also improve the system. Overall, our findings present a CRISPR-based amplification-free biosensor in designing a GO-TANF array integrated with CRISPR-Cas12a-based enzymatic cleavage, providing a promising approach for enhancing SERS signal intensity and improving sensitivity for numerous biomarker detection, including viral DNA, genomic DNA, and cfDNA.

METHODS/EXPERIMENTAL

Materials and Reagents. AuNPs with a diameter of 60 nm were purchased from BB International (Cardiff, UK). Cas12a enzyme and crRNA were obtained from IDT Korea (m.biotech, Seoul, Korea). Heterobifunctional ssDNA (NH_2-5′-ATATATATATA-3′-SH and NH_2-5′-ATATATATATA-3′-TAMRA), HBV DNA target and its crRNA (5′- TTGGCTTTCAGTTATATGGATGATGTGGTA3′, 5′-UAAUUUCUACUCUUGUAGAUUACCACAUCAUCCAUAUAAC-3′), HPV16L1 target and its crRNA (5′-GTGCTGCCATATCTACTTCA-3′, 5′-UAAUUUCUACUCUUGUAGAUUGAAGUAGAUAUGGCAGCAC-3′), HPV18L1 target and its crRNA (5′-TGTGTAGAAGCACATATTGT-3′, 5′-UAAUUUCUACUCUUGUAGAUACAAUAUGUGCUUCUACACA-3′) were synthesized from IDT Korea (m.biotech, Seoul, Korea). 5-TAMRA was obtained from ThermoFisher Scientific (Waltham, MA, USA). DNase I was purchased from Sigma-Aldrich (St. Louis, MO, USA). Gold (Au) and silver (Ag) plating solutions were obtained from Alfa Aesar (Haverhill, MA, USA). Polydimethylsiloxane was purchased from Dow Chemical (Midland, MI, USA). Nitric acid was obtained from Daejung (Seoul, Korea). 4-(2-Hydroxyethyl)-1-piperazineethanesulfonic acid (HEPES) buffer solution (20 mM) was obtained from Sigma-Aldrich. Phosphate-buffered saline (PBS; pH 7.4, 15 mM) solution was purchased from Sigma-Aldrich. Each of these solutions had a pH of 7.4, which mimics physiological pH. Deionized (DI) water, obtained from a Millipore

https://doi.org/10.1021/acsnano.1c03975
ACS Nano 2021, 15, 13475−13485

water system, was used throughout the experiments. All other chemicals were analytical-grade reagents.

Development of the GO-TANF Array. The triangle Au microstructure was fabricated by photolithography on the silicon substrate (National Nanofab Center, Korea). For the adhesion of Au on a silicon substrate, Ti was deposited at a 20 nm thickness, and Au was deposited at 200 nm. The length of one side of an equilateral triangle was 50 μm, and the overlaid equilateral triangle consisted of three 1 μm-sized sides. Au substrates were sonicated with 1% Triton X-100, DI water, and 95% ethanol for 20 min each and dried with N_2 gas. Next, Au and Ag electrodeposition solutions were mixed and electrodeposited on the triangle Au microstructure by the μAutolab electrochemical machine. The applied voltage was −0.95 mV, and the total quantity of electricity was −10 C. After the electrodeposition, the Au−Ag co-deposited substrate was washed with 0.1 M PBS, 0.05% Tween 20, and 0.1% bovine serum albumin (BSA). To eliminate Ag, the Au−Ag co-deposited substrate was placed in a 20% nitric acid (HNO_3) solution (mixed with DI water) for 5 min. For washing the residues, the TANF array was washed with ethanol and DI water. For the modification of the GO on the TANF array, a 1 mM cysteamine solution was covered on the whole substrate for 180 min and washed three times with DI water. Afterward, a GO solution (Sigma-Aldrich, USA) was placed on the TANF array and incubated overnight at room temperature (RT).

Functionalization of RAuNPs on the GO-TANF Array. The 60 nm-sized AuNPs (1 OD) were functionalized with 5-TAMRA (1 mg/mL) by physical adsorption for 1 h at RT. 5-TAMRA is a fluorescent Raman probe used for making Raman-active nanoprobes (RAuNP). After functionalization, heterobifunctional ssDNA was incubated on a rocking shaker for 1 h at RT to create a coating on the RAuNP surface by Au thiol interaction. For the prevention of nonspecific reaction, 3% BSA was added to the RAuNP solution overnight at 4 °C. After several washing steps (10 min at 10 000 rpm, resuspension in PBS, 0.05% Tween 20, 0.1% BSA) to eliminate residual ssDNA, they were resuspended in PBS and 0.05% Tween 20 and kept at 4 °C. After ssDNA immobilization, the ssDNA-functionalized RAuNP was applied to the GO-TANF array to connect the RAuNP and GO-TANF using the NH_2−GO interaction for 3 h at RT.

FTDT Simulation of Electromagnetic and Chemical Enhancement on the RAuNP-Functionalized GO-TANF Array. We studied the enhancement of the EM for the SERS experiment. Specifically, we performed an FDTD simulation based on parameters mimicking the real structures characterized by SEM. Briefly, 3D models for an individual Au nanoflower structure were built (symmetrically assembled from six parabola cone structures with heights of 250 nm) with the composition of gold [Re(index) = 0.08 and Im(index) = 4.56 at a wavelength of 780 nm]. Then we built arrays of individual structures on a silicon substrate [Re(index) = 3.714 and Im(index) = 0.008]. Afterward, we performed the FDTD simulation using a mesh size of 4 nm combined with a perfectly matched layer boundary condition (layer number: 12). Vacuum conditions were used as the media for the FDTD simulation. The parallel and vertical monitors were positions at assigned planes. To simulate the EM field for gold nanoparticle-derived structures, the same mesh size, material setting, and boundary conditions were used. We generated and plotted E/E_0 as a function of the positions on the monitor planes in OriginLab.

Electrophoresis. Degradation of ssDNA and target DNA was investigated with native tris-borate-EDTA (TBE) native polyacrylamide gel electrophoresis (PAGE). Target DNA (HPV), ssDNA, ssDNA with DNase I, and ssDNA with activated CRISPR-Cas12a were confirmed by native TBE PAGE stained by ethidium bromide for 10 min, and images were taken.

Detection of Viral DNAs by Using the Activated CRISPR-Cas12a Complex on the RAuNP-Functionalized GO-TANF Array. The three-by-three PDMS well chamber was first attached to the surface of the GO-TANF array after plasma treatment for 5 min. For the activated CRISPR-Cas12a complex, 30 nM Cas12a and 30 nM crRNA were reacted in the RNase free water for 10 min at 37 °C. After forming the CRISPR-Cas12a complex, target DNA was applied to the CRISPR-Cas12a complex in cleavage buffer (20 mM HEPES, 150 mM KCl, 10 mM $MgCl_2$, 1% glycerol, and 0.5 mM dithiothreitol). The activated solution was put on the RAuNP-functionalized GO-TANF array for 20 min at RT. The SERS signal intensity was determined by Raman NTEGRA spectra with a liquid nitrogen-cooled CCD detector. The XY scan range was varied, from 50 μm × 50 to 100 μm × 100 μm; the resolution of the spectrometer was 785 nm in the XYZ plane; the mapping points were 32 × 32. Raman spectra were recorded using a NIR laser-emitting light at a wavelength of 785 nm, with an irradiation laser power of 3 mW on the sample plane. The activated CRISPR-Cas12a solution was removed, and the substrates were washed three times with PBS before SERS measurements to eliminate the effect of the separated RAuNP on SERS signals. Ten scans of 1 s exposure from 300 to 1800 cm^{-1} were recorded, and the mean result was used. A blank spectrum was acquired before each step, which allowed the absorbance to be subsequently measured.

ASSOCIATED CONTENT

Supporting Information

The Supporting Information is available free of charge at https://pubs.acs.org/doi/10.1021/acsnano.1c03975.

Materials and methods, design of triangle-patterned Au microstructure on the silicon substrate, schematic diagram of GO-modified TANF substrate by electrochemical deposition, SEM image of triangle Au microstructure, Au−Ag co-deposited alloy nanostructure, TANF structure and GO-TANF structure, preparation of DNA-functionalized 20- and 60-AuNP, TEM analysis for the confirmation of functionalization and binding formation of 20- and 60-AuNP, comparison of the Au nanostructure and Au nanoflower on the triangle Au microstructure by electrochemical deposition, SEM and EDS mapping images of Au nanostructure, Au−Ag alloy nanostructure, Au nanoflower, and GO-Au nanoflower, SERS enhancement effect of diverse Au-based nanostructures, SEM images of diverse Au nanostructures by Ag elimination method, Raman intensities of the D and G band of each Au nanostructure, Raman mapping and CRM images of NE-4C cells on a hybrid nano-SERS array with MG-DA aptamers, electrophoresis image of the target DNA, ssDNA, ssDNA with DNase treatment, and ssDNA with target and CRISPR-Cas12a complex, highly sensitive measurement of HBV DNA on the RAuNP-modified GO-TANF array by CRISPR-Cas12a-based ssDNA degradation, and the surface of GO-TANF substrate, Figures S1−S13 (PDF)

AUTHOR INFORMATION

Corresponding Authors

Ki-Bum Lee − *Department of Chemistry and Chemical Biology, Rutgers, The State University of New Jersey, Piscataway, New Jersey 08854, United States;* orcid.org/0000-0002-8164-0047; Email: kblee@rutgers.edu

Jeong-Woo Choi − *Department of Chemical & Biomolecular Engineering, Sogang University, Seoul 04107, Republic of Korea;* orcid.org/0000-0003-0100-0582; Email: jwchoi@sogang.ac.kr

Authors

Jin-Ha Choi − *Department of Chemical & Biomolecular Engineering, Sogang University, Seoul 04107, Republic of Korea; School of Chemical Engineering, Jeonbuk National*

University, Jeonju, Jeollabuk-do 54896, Republic of Korea; orcid.org/0000-0002-1632-9586

Minkyu Shin − *Department of Chemical & Biomolecular Engineering, Sogang University, Seoul 04107, Republic of Korea*

Letao Yang − *Department of Chemistry and Chemical Biology, Rutgers, The State University of New Jersey, Piscataway, New Jersey 08854, United States;* orcid.org/0000-0002-0572-9787

Brian Conley − *Department of Chemistry and Chemical Biology, Rutgers, The State University of New Jersey, Piscataway, New Jersey 08854, United States*

Jinho Yoon − *Department of Chemical & Biomolecular Engineering, Sogang University, Seoul 04107, Republic of Korea; Department of Chemistry and Chemical Biology, Rutgers, The State University of New Jersey, Piscataway, New Jersey 08854, United States*

Sang-Nam Lee − *Uniance Gene Inc., Seoul 04107, Republic of Korea*

Complete contact information is available at: https://pubs.acs.org/10.1021/acsnano.1c03975

Author Contributions

J.-H.C. and J.-W.C. initially designed the concept. J.-H.C. and K.-B.L. organized the structure of the experimental design and manuscript. J.-H.C. and M.S. conducted all experiments. J.-H.C. and J.-W.C. wrote the first draft of the manuscript. L.Y., B.C., S.-N.L., K.-B.L., and J.Y. updated and revised the manuscript. All authors collaboratively completed the manuscript. All authors have read and agreed to the published version of the manuscript.

Notes

The authors declare no competing financial interest.

ACKNOWLEDGMENTS

This work was supported by the National Research Foundation of Korea (NRF) grant funded by the Korean government (MSIT) (2019R1A2C3002300), Basic Science Research Program through the NRF funded by the Ministry of Education (2016R1A6A1A03012845), and the NRF grant funded by the Korean government (MSIT) (2021R1F1A1061201). K.-B.L. acknowledges the partial financial support from the NSF (CBET-1803517) and New Jersey Health Foundation.

REFERENCES

(1) Hanna, T. P.; Evans, G. A.; Booth, C. M. Cancer, COVID-19 and the Precautionary Principle: Prioritizing Treatment during a Global Pandemic. *Nat. Rev. Clin. Oncol.* **2020**, *17* (5), 268−270.

(2) Zheng, J. SARS-CoV-2: An Emerging Coronavirus that Causes a Global Threat. *Int. J. Biol. Sci.* **2020**, *16* (10), 1678−1685.

(3) Lai, C.-C.; Shih, T.-P.; Ko, W.-C.; Tang, H.-J.; Hsueh, P.-R. Severe Acute Respiratory Syndrome Coronavirus 2 (SARS-CoV-2) and Corona Virus Disease-2019 (COVID-19): The Epidemic and the Challenges. *Int. J. Antimicrob. Agents* **2020**, *55*, 105924.

(4) Coronaviridae Study Group of the International Committee on Taxonomy of Viruses.. The Species Severe Acute Respiratory Syndrome-Related Coronavirus: Classifying 2019-nCoV and Naming It SARS-CoV-2. *Nat. Microbiol.* **2020**, *5* (4), 536.

(5) Lauer, S. A.; Grantz, K. H.; Bi, Q.; Jones, F. K.; Zheng, Q.; Meredith, H. R.; Azman, A. S.; Reich, N. G.; Lessler, J. The Incubation Period of Coronavirus Disease 2019 (COVID-19) from Publicly Reported Confirmed Cases: Estimation and Application. *Ann. Intern. Med.* **2020**, *172* (9), 577−582.

(6) Jiang, X.; Rayner, S.; Luo, M. H. Does SARS-CoV-2 Has a Longer Incubation Period than SARS and MERS? *J. Med. Virol.* **2020**, *92* (5), 476−478.

(7) Xu, Y.; Li, X.; Zhu, B.; Liang, H.; Fang, C.; Gong, Y.; Guo, Q.; Sun, X.; Zhao, D.; Shen, J.; Zhang, H.; Liu, H.; Xia, H.; Tang, J.; Zhang, K.; Gong, S. Characteristics of Pediatric SARS-CoV-2 Infection and Potential Evidence for Persistent Fecal Viral Shedding. *Nat. Med.* **2020**, *26* (4), 502−505.

(8) Yang, L.; Li, M.; Du, F.; Chen, G.; Yasmeen, A.; Tang, Z. A Novel Colorimetric PCR-Based Biosensor for Detection and Quantification of Hepatitis B Virus. In *Biosensors and Biodetection*; Springer, 2017; pp 357−369.

(9) Wang, R.; Zhao, X.; Chen, X.; Qiu, X.; Qing, G.; Zhang, H.; Zhang, L.; Hu, X.; He, Z.; Zhong, D.; Wang, Y.; Luo, Y. Rolling Circular Amplification (RCA)-Assisted CRISPR/Cas9 Cleavage (RACE) for Highly Specific Detection of Multiple Extracellular Vesicle MicroRNAs. *Anal. Chem.* **2020**, *92* (2), 2176−2185.

(10) Broughton, J. P.; Deng, X.; Yu, G.; Fasching, C. L.; Servellita, V.; Singh, J.; Miao, X.; Streithorst, J. A.; Granados, A.; Sotomayor-Gonzalez, A.; Zorn, K.; Gopez, A.; Hsu, E.; Gu, W.; Miller, S.; Pan, C. Y.; Guevara, H.; Wadford, D. A.; Chen, J. S.; Chiu, C. Y. CRISPR-Cas12-Based Detection of SARS-CoV-2. *Nat. Biotechnol.* **2020**, *38* (7), 870−874.

(11) Bao, Y.; Jiang, Y.; Xiong, E.; Tian, T.; Zhang, Z.; Lv, J.; Li, Y.; Zhou, X. CUT-LAMP: Contamination-Free Loop-Mediated Isothermal Amplification Based on the CRISPR/Cas9 Cleavage. *ACS Sens.* **2020**, *5* (4), 1082−1091.

(12) Zhou, W.; Hu, L.; Ying, L.; Zhao, Z.; Chu, P. K.; Yu, X. F. A CRISPR-Cas9-Triggered Strand Displacement Amplification Method for Ultrasensitive DNA Detection. *Nat. Commun.* **2018**, *9* (1), 5012.

(13) Chen, J. S.; Ma, E.; Harrington, L. B.; Da Costa, M.; Tian, X.; Palefsky, J. M.; Doudna, J. A. CRISPR-Cas12a Target Binding Unleashes Indiscriminate Single-Stranded DNase Activity. *Science* **2018**, *360* (6387), 436−439.

(14) Myhrvold, C.; Freije, C. A.; Gootenberg, J. S.; Abudayyeh, O. O.; Metsky, H. C.; Durbin, A. F.; Kellner, M. J.; Tan, A. L.; Paul, L. M.; Parham, L. A.; Garcia, K. F.; Barnes, K. G.; Chak, B.; Mondini, A.; Nogueira, M. L.; Isern, S.; Michael, S. F.; Lorenzana, I.; Yozwiak, N. L.; MacInnis, B. L.; Bosch, I.; Gehrke, L.; Zhang, F.; Sabeti, P. C. Field-Deployable Viral Diagnostics Using CRISPR-Cas13. *Science* **2018**, *360* (6387), 444−448.

(15) Gootenberg, J. S.; Abudayyeh, O. O.; Kellner, M. J.; Joung, J.; Collins, J. J.; Zhang, F. Multiplexed and Portable Nucleic Acid Detection Platform with Cas13, Cas12a, and Csm6. *Science* **2018**, *360* (6387), 439−444.

(16) Gootenberg, J. S.; Abudayyeh, O. O.; Lee, J. W.; Essletzbichler, P.; Dy, A. J.; Joung, J.; Verdine, V.; Donghia, N.; Daringer, N. M.; Freije, C. A.; Myhrvold, C.; Bhattacharyya, R. P.; Livny, J.; Regev, A.; Koonin, E. V.; Hung, D. T.; Sabeti, P. C.; Collins, J. J.; Zhang, F. Nucleic Acid Detection with CRISPR-Cas13a/C2c2. *Science* **2017**, *356* (6336), 438−442.

(17) Kellner, M. J.; Koob, J. G.; Gootenberg, J. S.; Abudayyeh, O. O.; Zhang, F. SHERLOCK: Nucleic Acid Detection with CRISPR Nucleases. *Nat. Protoc.* **2019**, *14* (10), 2986−3012.

(18) Li, S. Y.; Cheng, Q. X.; Wang, J. M.; Li, X. Y.; Zhang, Z. L.; Gao, S.; Cao, R. B.; Zhao, G. P.; Wang, J. CRISPR-Cas12a-Assisted Nucleic Acid Detection. *Cell Discovery* **2018**, *4* (1), 20.

(19) Zong, C.; Xu, M.; Xu, L. J.; Wei, T.; Ma, X.; Zheng, X. S.; Hu, R.; Ren, B. Surface-Enhanced Raman Spectroscopy for Bioanalysis: Reliability and Challenges. *Chem. Rev.* **2018**, *118* (10), 4946−4980.

(20) Novikov, S. M.; Boroviks, S.; Evlyukhin, A. B.; Tatarkin, D. E.; Arsenin, A. V.; Volkov, V. S.; Bozhevolnyi, S. I. Fractal Shaped Periodic Metal Nanostructures Atop Dielectric-Metal Substrates for SERS Applications. *ACS Photonics* **2020**, *7* (7), 1708−1715.

(21) Nehra, K.; Pandian, S. K.; Bharati, M. S. S.; Soma, V. R. Enhanced Catalytic and SERS Performance of Shape/Size Controlled Anisotropic Gold Nanostructures. *New J. Chem.* **2019**, *43* (9), 3835−3847.

(22) El-Said, W. A.; Yoon, J.; Choi, J. W. Nanostructured Surfaces for Analysis of Anticancer Drug and Cell Diagnosis Based on Electrochemical and SERS Tools. *Nano Converg.* **2018**, *5* (1), 11.
(23) Hussein, M. A.; El-Said, W. A.; Abu-Zied, B. M.; Choi, J. W. Nanosheet Composed of Gold Nanoparticle/Graphene/Epoxy Resin Based on Ultrasonic Fabrication for Flexible Dopamine Biosensor Using Surface-Enhanced Raman Spectroscopy. *Nano Converg.* **2020**, *7* (1), 1−12.
(24) Kneipp, K.; Wang, Y.; Kneipp, H.; Perelman, L. T.; Itzkan, I.; Dasari, R.; Feld, M. S. Single Molecule Detection Using Surface-Enhanced Raman Scattering (SERS). *Phys. Rev. Lett.* **1997**, *78* (9), 1667−1670.
(25) Choi, J. H.; Kim, T. H.; El-Said, W. A.; Lee, J. H.; Yang, L. T.; Conley, B.; Choi, J. W.; Lee, K. B. *In Situ* Detection of Neurotransmitters from Stem Cell-Derived Neural Interface at the Single-Cell Level *via* Graphene-Hybrid SERS Nanobiosensing. *Nano Lett.* **2020**, *20* (10), 7670−7679.
(26) Yang, L. T.; Lee, J. H.; Rathnam, C.; Hou, Y. N.; Choi, J. W.; Lee, K. B. Dual-Enhanced Raman Scattering-Based Characterization of Stem Cell Differentiation Using Graphene-Plasmonic Hybrid Nanoarray. *Nano Lett.* **2019**, *19* (11), 8138−8148.
(27) Choi, J. H.; El-Said, W. A.; Choi, J. W. Highly Sensitive Surface-Enhanced Raman Spectroscopy (SERS) Platform Using Core/Double Shell (Ag/Polymer/Ag) Nanohorn for Proteolytic Biosensor. *Appl. Surf. Sci.* **2020**, *506*, 144669.
(28) Kim, H.; Lee, S.; Seo, H. W.; Kang, B.; Moon, J.; Lee, K. G.; Yong, D.; Kang, H.; Jung, J.; Lim, E. K.; Jeong, J. Clustered Regularly Interspaced Short Palindromic Repeats-Mediated Surface-Enhanced Raman Scattering Assay for Multidrug-Resistant Bacteria. *ACS Nano* **2020**, *14* (12), 17241−17253.
(29) Huang, S.; Pandey, R.; Barman, I.; Kong, J.; Dresselhaus, M. Raman Enhancement of Blood Constituent Proteins Using Graphene. *ACS Photonics* **2018**, *5* (8), 2978−2982.
(30) Liu, D.; Chen, X.; Hu, Y.; Sun, T.; Song, Z.; Zheng, Y.; Cao, Y.; Cai, Z.; Cao, M.; Peng, L.; Huang, Y. Raman Enhancement on Ultra-Clean Graphene Quantum Dots Produced by Quasi-Equilibrium Plasma-Enhanced Chemical Vapor Deposition. *Nat. Commun.* **2018**, *9* (1), 1−10.
(31) Ling, X.; Xie, L.; Fang, Y.; Xu, H.; Zhang, H.; Kong, J.; Dresselhaus, M. S.; Zhang, J.; Liu, Z. Can Graphene Be Used as a Substrate for Raman Enhancement? *Nano Lett.* **2010**, *10*, 553−561.
(32) Barros, E. B.; Dresselhaus, M. S. Theory of Raman Enhancement by Two-Dimensional Materials: Applications for Graphene-Enhanced Raman Spectroscopy. *Phys. Rev. B: Condens. Matter Mater. Phys.* **2014**, *90*, 035443.
(33) Jeong, J. W.; Arnob, M. M. P.; Baek, K. M.; Lee, S. Y.; Shih, W. C.; Jung, Y. S. 3D Cross-Point Plasmonic Nanoarchitectures Containing Dense and Regular Hot Spots for Surface-Enhanced Raman Spectroscopy Analysis. *Adv. Mater.* **2016**, *28* (39), 8695−8704.
(34) Liu, K.; Bai, Y.; Zhang, L.; Yang, Z.; Fan, Q.; Zheng, H.; Yin, Y.; Gao, C. Porous Au−Ag Nanospheres with High-Density and Highly Accessible Hot-Spots for SERS Analysis. *Nano Lett.* **2016**, *16* (6), 3675−3681.
(35) Bruch, R.; Baaske, J.; Chatelle, C.; Meirich, M.; Madlener, S.; Weber, W.; Dincer, C.; Urban, G. A. CRISPR/Cas13a-Powered Electrochemical Microfluidic Biosensor for Nucleic Acid Amplification-Free miRNA Diagnostics. *Adv. Mater.* **2019**, *31* (51), No. e1905311.
(36) Dai, Y.; Somoza, R. A.; Wang, L.; Welter, J. F.; Li, Y.; Caplan, A. I.; Liu, C. C. Exploring the Trans-Cleavage Activity of CRISPR-Cas12a (cpf1) for the Development of a Universal Electrochemical Biosensor. *Angew. Chem., Int. Ed.* **2019**, *58* (48), 17399−17405.
(37) Hajian, R.; Balderston, S.; Tran, T.; deBoer, T.; Etienne, J.; Sandhu, M.; Wauford, N. A.; Chung, J. Y.; Nokes, J.; Athaiya, M.; Paredes, J.; Peytavi, R.; Goldsmith, B.; Murthy, N.; Conboy, I. M.; Aran, K. Detection of Unamplified Target Genes *via* CRISPR-Cas9 Immobilized on a Graphene Field-Effect Transistor. *Nat. Biomed. Eng.* **2019**, *3* (6), 427−437.
(38) Shan, Y.; Zhou, X.; Huang, R.; Xing, D. High-Fidelity and Rapid Quantification of miRNA Combining crRNA Programmability and CRISPR/Cas13a trans-Cleavage Activity. *Anal. Chem.* **2019**, *91* (8), 5278−5285.
(39) Xu, W.; Jin, T.; Dai, Y.; Liu, C. C. Surpassing the Detection Limit and Accuracy of the Electrochemical DNA Sensor Through the Application of CRISPR Cas Systems. *Biosens. Bioelectron.* **2020**, *155*, 112100.
(40) Zhou, T.; Huang, R.; Huang, M. Q.; Shen, J. J.; Shan, Y. Y.; Xing, D. CRISPR/Cas13a Powered Portable Electrochemiluminescence Chip for Ultrasensitive and Specific MiRNA Detection. *Adv. Sci.* **2020**, *7* (13), 1903661.
(41) Bruch, R.; Johnston, M.; Kling, A.; Mattmuller, T.; Baaske, J.; Partel, S.; Madlener, S.; Weber, W.; Urban, G. A.; Dincer, C. CRISPR-Powered Electrochemical Microfluidic Multiplexed Biosensor for Target Amplification-Free MiRNA Diagnostics. *Biosens. Bioelectron.* **2021**, *177*, 112887.
(42) Choi, J. H.; Lim, J.; Shin, M.; Paek, S. H.; Choi, J. W. CRISPR-Cas12a-Based Nucleic Acid Amplification-Free DNA Biosensor *via* Au Nanoparticle-Assisted Metal-Enhanced Fluorescence and Colorimetric Analysis. *Nano Lett.* **2021**, *21* (1), 693−699.
(43) Lee, Y.; Choi, J.; Han, H.-K.; Park, S.; Park, S. Y.; Park, C.; Baek, C.; Lee, T.; Min, J. Fabrication of Ultrasensitive Electrochemical Biosensor for Dengue Fever Viral RNA Based on CRISPR/Cpf1 Reaction. *Sens. Actuators, B* **2021**, *326*, 128677.
(44) Liu, P. F.; Zhao, K. R.; Liu, Z. J.; Wang, L.; Ye, S. Y.; Liang, G. X. Cas12a-Based Electrochemiluminescence Biosensor for Target Amplification-free DNA Detection. *Biosens. Bioelectron.* **2021**, *176*, 112954.
(45) Tian, T.; Shu, B.; Jiang, Y.; Ye, M.; Liu, L.; Guo, Z.; Han, Z.; Wang, Z.; Zhou, X. An Ultralocalized Cas13a Assay Enables Universal and Nucleic Acid Amplification-Free Single-Molecule RNA Diagnostics. *ACS Nano* **2021**, *15* (1), 1167−1178.

https://doi.org/10.1021/acsnano.1c03975
ACS Nano 2021, 15, 13475−13485